Birefringence Simulations of Calcium Fluoride Single Crystal Used as Chamber Window of Gas Laser Light Source

Yuta Kitamura[1], Noriyuki Miyazaki[1], Takahito Kumazaki[2]
Naoto Nagakura[3], Yasuhiro Hashimoto[3] and Isao Masada[3]

Abstract: CaF_2 single crystal is used as high performance optical elements. We developed an analysis system for simulating birefringence of CaF_2 single crystal used as a chamber window of a gas laser light source. The analysis system consists of a stress analysis and a birefringence analysis. In the stress analysis, the finite element method was applied to obtain the mechanical stress caused by a window holder and gas pressure. In the birefringence analysis, the photo-elastic effect gives the change of refractive indices, from which the optical path difference and the fast axis are calculated by using the average stress method. The crystal anisotropy of CaF_2 single crystal was taken into account in these analyses. We can perform a birefringence simulation for a chamber window of CaF_2 single crystal with any crystal direction and any incident direction, using this analysis system. We performed the analyses of a crystal with a surface vertical to the <111> direction under the Brewster's angle of incidence and several rotation angles. From these analyses, we obtained reasonable results of the optical path difference and the fast axis in comparison with experimental results.

Keywords: Birefringence, Finite element methods, Calcium compounds, Numerical analysis.

1   Introduction

Calcium fluoride (hereafter abbreviated as CaF_2) single crystal has high durability and excellent transmission characteristics down to the vacuum ultraviolet region. Because of this reason, CaF_2 single crystal is used as a chamber window material

---

[1] Department of Mechanical Engineering and Science, Kyoto University, Kyoto, 606-8501, Japan

[2] Development Division, Gigaphoton INC., Tochigi, 323-8558, Japan

[3] CF-10 Department, Research and Development Division, Tokuyama Corporation, Yamaguchi, 745-8648, Japan

of gas laser light sources, which is needed especially higher durability than other optical elements for semiconductor lithography, instead of conventional synthetic quartz.

Extremely high material performances are required for window materials to achieve high efficiency and quality of gas laser light sources. In such use of CaF_2 single crystal, one of the technical issues is birefringence caused by the photo-elastic effect due to the stress in the crystal. Such birefringence results in degrading optical quality of CaF_2 single crystal. When CaF_2 single crystal is used as a chamber window of a gas laser light source, mechanical stresses are induced in the chamber window by mechanical loads, as shown in Fig. 1. The window is fixed with the window holder tightened by bolts and the O-rings are set both on the upper and lower surfaces of the single crystal window not to leak laser gas and purge gas. The window is subjected to loads through these O-rings. In addition, both faces of the window are subjected to laser gas pressure and purge gas pressure, respectively. Such loads and gas pressures induce stresses in the window. These stresses cause the birefringence and lead to performance degradation. Gas laser enters into the window with the Brewster's angle. This is because the Brewster's angle of incidence makes no reflection of p-polarization, a polarization component parallel to a plane of incidence. When the angle of incidence is not zero, birefringence is changed by the incident direction relative to the crystal orientation. These factors make the birefringence phenomenon more complicated. Therefore, the use of simulation technique is more effective than experiment in order to search the optimum condition for window design of laser equipment.

As for birefringence analyses of CaF_2 single crystal, several papers have been already published. Abbott, Wang, Price, Allan, and Slater (2003) performed a birefringence analysis of CaF_2 single crystal after crystal annealing. In their analysis, they used an approximate method using the average values of stresses along the optical path (hereafter this method is called the average stress method). Schmid, Weber, Graf, Roos, and Weber (2000) applied the Jones calculus, the exact method for the birefringence calculation, to the thermally induced birefringence in Nd:Yag crystal laser rods. In our previous paper [Ogino, Miyazaki, Mabuchi, and Nawata (2008)], we developed a methodology for simulating the birefringence of an annealed ingot of the <001>-growth CaF_2 single crystal, and also clarified the relation between the approximate method for birefringence calculation, i.e. the average stress method and the Jones calculus in anisotropic materials. Then we performed the birefringence analysis of the <001>-growth CaF_2 single crystal after annealing by using a stress-free temperature proposed by Abbott, Wang, Price, Allan, and Slater (2003) to obtain residual stress after ingot annealing, which makes residual stress calculation possible with an elastic thermal stress analysis. We also per-

formed a nonlinear finite element analysis using a creep constitutive equation for CaF_2 single crystal to obtain the residual stress after ingot annealing without assuming a stress-free temperature [Miyazaki, Ogino, Kitamura, Mabuchi, and Nawata (2009)].

In the present study, we performed birefringence simulations for a CaF_2 single crystal chamber window used in a gas laser light source, which has the surfaces vertical to the <111> direction of the crystal. We considered several incident directions of light and compared these analytical results with experimental results.
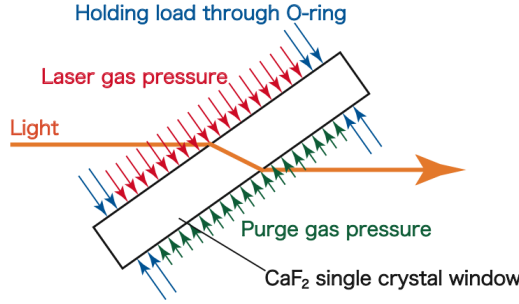
Figure 1: Mechanical loads acting on a CaF_2 single crystal chamber window of a gas laser light source

2 Theory of birefringence

Based on the reference [Nye (1985)], we summarize the theory of birefringence.

2.1 Photo-elastic effect

The dielectric constant is changed by the stress. Such an effect is called the photo-elastic effect. In general, it is given by

$$\begin{Bmatrix} \Delta B_1 \\ \Delta B_2 \\ \Delta B_3 \\ \Delta B_4 \\ \Delta B_5 \\ \Delta B_6 \end{Bmatrix} = \begin{bmatrix} \pi_{11} & \pi_{12} & \pi_{13} & \pi_{14} & \pi_{15} & \pi_{16} \\ \pi_{21} & \pi_{22} & \pi_{23} & \pi_{24} & \pi_{25} & \pi_{26} \\ \pi_{31} & \pi_{32} & \pi_{33} & \pi_{34} & \pi_{35} & \pi_{36} \\ \pi_{41} & \pi_{42} & \pi_{43} & \pi_{44} & \pi_{45} & \pi_{46} \\ \pi_{51} & \pi_{52} & \pi_{53} & \pi_{54} & \pi_{55} & \pi_{56} \\ \pi_{61} & \pi_{62} & \pi_{63} & \pi_{64} & \pi_{65} & \pi_{66} \end{bmatrix} \begin{Bmatrix} \sigma_1 \\ \sigma_2 \\ \sigma_3 \\ \sigma_4 \\ \sigma_5 \\ \sigma_6 \end{Bmatrix} \tag{1}$$

where σ_i is the stress, ΔB_i is the change of the inverse dielectric constant and π_{ij} is the piezo-optical constant. The subscripts i and j are abbreviated forms of tensor

indices, and the corresponding relations are as follows: $11 \rightarrow 1$, $22 \rightarrow 2$, $33 \rightarrow 3$, 23 and $32 \rightarrow 4$, 31 and $13 \rightarrow 5$, and 12 and $21 \rightarrow 6$.

For a cubic single crystal such as CaF_2, the piezo-optical matrix can be simplified as follows, when the analysis coordinate system is coincident with the crystal coordinate system:

$$
\begin{bmatrix}
\pi_{11} & \pi_{12} & \pi_{12} & 0 & 0 & 0 \\
& \pi_{11} & \pi_{12} & 0 & 0 & 0 \\
& & \pi_{11} & 0 & 0 & 0 \\
& & & \pi_{44} & 0 & 0 \\
& \text{Sym.} & & & \pi_{44} & 0 \\
& & & & & \pi_{44}
\end{bmatrix}
\tag{2}
$$

In the case where the analysis coordinate system is not coincident with the crystal coordinate system, the components of piezo-optical matrix are obtained using tensor transformation. The relationship between the tensor components of the piezo-optical constant in the crystal coordinate system π_{ijkl} and those in the analysis coordinate system π'_{ijkl} is given as follows:

$$
\pi'_{ijkl} = a_{im}a_{jn}a_{ko}a_{lp}\pi_{mnop}
\tag{3}
$$

where $a_{\alpha\beta}$ is given by

$$
a_{\alpha\beta} = \mathbf{e}'_{\alpha} \cdot \mathbf{e}_{\beta}
\tag{4}
$$

In the above equation, $\mathbf{e}'_{\alpha}$ and $\mathbf{e}_{\beta}$ are the base vectors of x'_{α}-coordinate and x_{β}-coordinate, respectively.

The inverse dielectric constant without stress B_i is express by the refractive index n as follows:

$$
\begin{Bmatrix}
B_1 \\
B_2 \\
B_3 \\
B_4 \\
B_5 \\
B_6
\end{Bmatrix}
=
\begin{Bmatrix}
B_1 \\
B_1 \\
B_1 \\
0 \\
0 \\
0
\end{Bmatrix}
=
\begin{Bmatrix}
1/n^2 \\
1/n^2 \\
1/n^2 \\
0 \\
0 \\
0
\end{Bmatrix}
\tag{5}
$$

2.2 Indicatrix

We consider the following indicatrix described in an analysis coordinate system $(x_1 - x_2 - x_3)$ to obtain the refractive indices:

$$
B_1 x_1^2 + B_2 x_2^2 + B_3 x_3^2 + 2B_4 x_2 x_3 + 2B_5 x_3 x_1 + 2B_6 x_1 x_2 = 1
\tag{6}
$$

When stress is applied to a single crystal, the indicatrix is expressed by adding the increment of B_i calculated from Eq. 1.

$$(B_1 + \Delta B_1) x_1^2 + (B_2 + \Delta B_2) x_2^2 + (B_3 + \Delta B_3) x_3^2$$
$$+ 2 (B_4 + \Delta B_4) x_2 x_3 + 2 (B_5 + \Delta B_5) x_3 x_1 + 2 (B_6 + \Delta B_6) x_1 x_2 = 1 \tag{7}$$

The refractive indices are determined as follows. As shown in Fig. 2, a wave surface cuts an ellipse from the ellipsoid. Light can be decomposed into the oscillation components along the two principal axes, that is, the long axis and the short axis, of the ellipse. The long axis and the short axis are called the slow axis and the fast axis, respectively. The lengths of the principal axes of the ellipse correspond to the refractive index along the slow axis n_s and that along the fast axis n_f, respectively.

When the wave normal coincides with the x_3-axis of the analysis coordinate system, the following equation is obtained by considering Eq. 5 and taking $x_3 = 0$ in Eq. 7:

$$(B_1 + \Delta B_1) x_1^2 + (B_1 + \Delta B_2) x_2^2 + 2 \Delta B_6 x_1 x_2 = 1 \tag{8}$$

From this ellipse, we can calculate the birefringence $\Delta n = n_s - n_f$ defined by the difference between two refractive indices and the azimuth ρ defined by the angle between the fast axis and the x_1-axis as follows:

$$\Delta n = \frac{1}{2} \left(B_1 + \frac{\Delta B_1 + \Delta B_2}{2} \right)^{-3/2} \sqrt{(\Delta B_1 - \Delta B_2)^2 + 4 \Delta B_6^2} \tag{9}$$

$$\tan 2\rho = \frac{2 \Delta B_6}{\Delta B_1 - \Delta B_2} \tag{10}$$
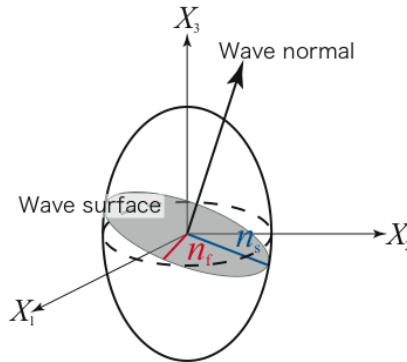
Figure 2: An indicatrix and determination of refractive indices

3 Method of analysis

In the birefringence simulation of CaF$_2$ single crystal used for the chamber window of the gas laser light source shown in Fig. 1, the stress analysis was first performed and we obtained the stress caused by the mechanical loads. Then the optical path difference and the azimuth were calculated based on the stress in the single crystal.

3.1 Stress analysis

Finite element method is used for many analysis [Brocks and Qi (2002); Nishioka and Stan (2003); Mittal (2008)] .We performed the stress analysis of CaF$_2$ single crystal by using a finite element computer code MSC MARC [MSC Software (2007)], because cubic single crystal CaF$_2$ has crystal anisotropy in the elastic constant. In this analysis, we obtained the stress caused by the mechanical loads from the window holder and the gas pressures.

3.2 Birefringence analysis

In the present study, we used a circular slab ingot, as shown in Fig. 3, in which a stress distribution exists. The stress changes continuously along the normal direction of the wave surface of light, so that the birefringence also changes continuously along the wave normal direction.

An exact method for calculating the optical path difference and the azimuth is the Jones calculus [Kliger, Lewis, and Randall (1990)]. It requires a lot of layers along the thickness direction of the slab. A simple method called the average stress method was proposed [Abbott, Wang, Price, Allan, and Slater (2003)]. In their method, the stress components averaged along the wave normal are utilized to calculate the birefringence without dividing the ingot into a multi-layer system. When we define l-axis as the wave normal direction, the average stress along the wave normal $\bar{\sigma}_i$ is calculated as follows by using the stress σ_i:

$$\bar{\sigma}_i = \frac{1}{L} \int_0^L \sigma_i \mathrm{d}l \tag{11}$$

where L denotes the length of light passing in a slab ingot. Then the change of the inverse dielectric constant is given by

$$
\begin{Bmatrix} \Delta\bar{B}_1 \\ \Delta\bar{B}_2 \\ \Delta\bar{B}_3 \\ \Delta\bar{B}_4 \\ \Delta\bar{B}_5 \\ \Delta\bar{B}_6 \end{Bmatrix}
=
\begin{bmatrix}
\pi_{11} & \pi_{12} & \pi_{13} & \pi_{14} & \pi_{15} & \pi_{16} \\
\pi_{21} & \pi_{22} & \pi_{23} & \pi_{24} & \pi_{25} & \pi_{26} \\
\pi_{31} & \pi_{32} & \pi_{33} & \pi_{34} & \pi_{35} & \pi_{36} \\
\pi_{41} & \pi_{42} & \pi_{43} & \pi_{44} & \pi_{45} & \pi_{46} \\
\pi_{51} & \pi_{52} & \pi_{53} & \pi_{54} & \pi_{55} & \pi_{56} \\
\pi_{61} & \pi_{62} & \pi_{63} & \pi_{64} & \pi_{65} & \pi_{66}
\end{bmatrix}
\begin{Bmatrix} \bar{\sigma}_1 \\ \bar{\sigma}_2 \\ \bar{\sigma}_3 \\ \bar{\sigma}_4 \\ \bar{\sigma}_5 \\ \bar{\sigma}_6 \end{Bmatrix}
\tag{12}
$$

The birefringence $\Delta\bar{n}$ and the azimuth $\bar{\rho}$ are obtained by taking $\Delta\bar{B}_i$ in Eqs. 9 and 10.

$$\Delta\bar{n} = \frac{1}{2}\left(B_1 + \frac{\Delta\bar{B}_1 + \Delta\bar{B}_2}{2}\right)^{-3/2}\sqrt{(\Delta\bar{B}_1 - \Delta\bar{B}_2)^2 + 4\Delta\bar{B}_6^2} \tag{13}$$

$$\tan 2\bar{\rho} = \frac{2\Delta\bar{B}_6}{\Delta\bar{B}_1 - \Delta\bar{B}_2} \tag{14}$$

Then the optical path difference $\bar{\Gamma}$ is expressed as follows:

$$\begin{aligned}\bar{\Gamma} &= L\Delta\bar{n} \\ &= \frac{L}{2}\left(B_1 + \frac{\Delta\bar{B}_1 + \Delta\bar{B}_2}{2}\right)^{-3/2}\sqrt{(\Delta\bar{B}_1 - \Delta\bar{B}_2)^2 + 4\Delta\bar{B}_6^2}\end{aligned} \tag{15}$$

If we assume $B_1 \gg \Delta B_1, \Delta B_2$, Eq. 15 becomes as follows by considering Eqs. 1 and 2:

$$\begin{aligned}\bar{\Gamma} &= B_1^{-3/2}L\sqrt{(\Delta\bar{B}_1 - \Delta\bar{B}_2)^2 + 4\Delta\bar{B}_6^2} \\ &= B_1^{-3/2}L\sqrt{(\pi_{11} - \pi_{12})^2(\bar{\sigma}_1 - \bar{\sigma}_2)^2 + 4(\pi_{44}\bar{\sigma}_4)^2}\end{aligned} \tag{16}$$

The optical path difference can be calculated from the average stress components. According to our previous paper [Ogino, Miyazaki, Mabuchi, and Nawata (2008)], the average stress method is accurate enough in comparison with the Jones calculus when the order of stress is less than 10^9Pa. As shown later, the stress in the ingot satisfies this condition in the present study. The results of optical path difference are shown by the optical path difference per unit length $\bar{\Gamma}_{unit}$ as follows:

$$\bar{\Gamma}_{\text{unit}} = \frac{\bar{\Gamma}}{L} \tag{17}$$

4 Analysis conditions

4.1 Finite element mesh and crystal orientation

We used a circular slab ingot as shown in Fig. 3. The ingot is 50mm in diameter and 7mm in thickness. The figure also shows the finite element mesh used in the stress analysis. We used the twenty-noded isoparametric element. The finite element model has 3108 elements and 14055 nodes. In this ingot, the <111> direction of the crystal corresponds to the x_3-axis of the analysis coordinate system, which is the thickness direction as shown in Fig. 4. In addition, the <110> direction coincides with the x_1-axis in the $x_1 - x_2$ plane.
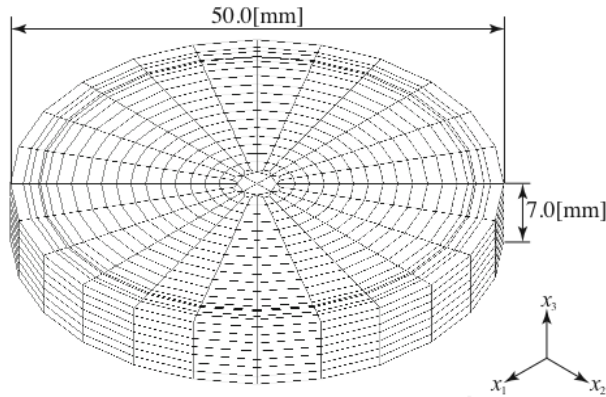
Figure 3: A circular slab ingot and its finite element mesh
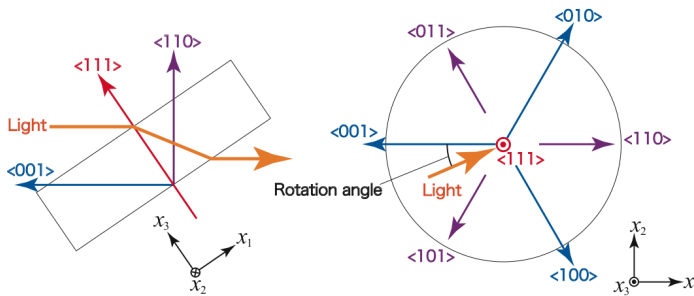
Figure 4: Crystal orientation of the analysis model

4.2   *Incident direction of light*

The wavelength of light is 633nm and the angle of incidence is the Brewster's angle 55.7° as shown in Fig. 5. The rotation angle is defined by the angle between the wave normal direction of the light and the <001> direction of the crystal in the $x_1 - x_2$ plane as shown in Fig. 4. We performed the analyses for the rotation angle of $\theta = 0$, 30 and 60°. Figure 5 also shows a coordinate system of the light axis $(u_1 - u_2 - u_3)$. As shown later, the results of birefringence analysis are represented by this coordinate system.

4.3   *Mechanical load*

We showed the mechanical loads applied to the CaF_2 single crystal used as the chamber window of the gas laser light source in Fig. 1. We considered the holding
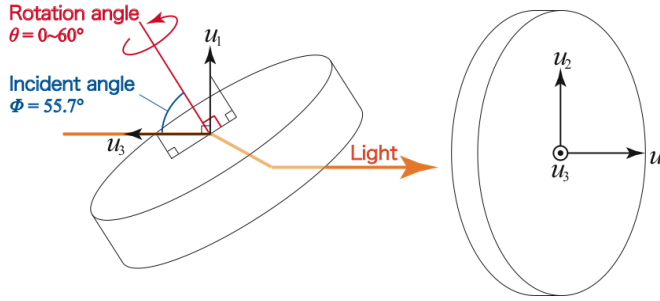
Figure 5: Rotation angle, angle of incidence and definition of a coordinate system of the light axis ($u_1 - u_2 - u_3$)

load through the O-rings and the pressure loads from laser gas and purge gas. One O-ring and the laser gas are in touch with the upper surface of the circular slab ingot. The other O-ring and the purge gas are in touch with the lower surface. These contact areas on the window are summarized in Tab. 1. The holding load measured by a torque wrench is 265N, the laser gas pressure is 400kPa and the purge gas pressure is 100kPa.

Table 1: The areas contacting on CaF_2 single crystal window

	External radius [mm]	Internal radius [mm]	Contact area [mm^2]
Upper O-ring	23.1	21.4	238
Lower O-ring	23.7	20.3	470
Gas	22.25	0.0	1555

4.4 Material property

For the stress analysis of a single crystal ingot, we need the elastic constants of CaF_2 single crystal. The data given in the reference [Vidal (1974)] were used to obtain the temperature dependence of elastic constants C_{11}, C_{12} and C_{44}. They are summarized in Tab. 2.

In the calculation of the optical path difference and the azimuth for CaF_2 single crystal, we need the piezo-optical coefficients π_{11}, π_{12} and π_{44}, which were quoted from the reference [Nye (1985)]. A refractive index n is also required to calculate $B_1 = B_2 (= 1/n^2)$, and we used a value given in a catalog [Schott Lithotec]. They are summarized in Tab. 3.

Table 2: Material properties of CaF$_2$ single crystal for stress analysis (Unit of T: K)

Elastic constants [Pa]	C_{11}	$-2.089 \times 10^7 T + 1.657 \times 10^{11}$
	C_{12}	$-3.282 \times 10^6 T + 4.565 \times 10^{10}$
	C_{44}	$-1.024 \times 10^7 T + 3.394 \times 10^{10}$

Table 3: Material properties of CaF$_2$ single crystal for birefringence analysis

Piezo-optical constants [Pa^{-1}]	π_{11}	-0.29×10^{-12}
	π_{12}	1.16×10^{-12}
	π_{44}	0.698×10^{-12}
Refractive index	n	1.43380
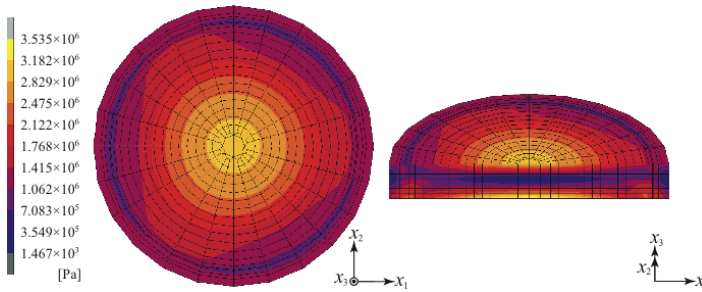
Figure 6: Distribution of von Mises equivalent stress obtained by the analysis

5 Results and discussion

We performed the analyses by using the conditions described above. First of all, we will show the result of the stress analysis considering the mechanical loads at the temperature of 293K. Figure 6 shows the distribution of von Mises equivalent stress for the single crystal window obtained by the analysis. In the $x_1 - x_2$ plane, we can recognize a three-fold symmetry of the equivalent stress distribution caused by the anisotropy of the elastic constants. We can find from this figure that the stress is the highest at the center of the upper and lower surfaces. It is also found that the stress changes along the thickness and becomes the highest at the upper and lower surfaces and almost zero at the mid plane. This means that the dominant factor for the stress in the single crystal window is the bending moment caused by the difference of the pressure between laser gas and purge gas. The stress caused by the holding loads through the O-rings is large toward the thickness direction in the contact area, but is attenuated significantly toward the radial direction and has

less influence for the photo-elastic effect at the area where light enters.

Next, we will show the results of the birefringence analysis obtained from the result of the stress analysis. As shown in Fig. 6, the order of the residual stress is 10^6MPa, so that the average stress method for the birefringence calculation is accurate enough. We performed the birefringence calculation for the circular region of 25mm in diameter on the upper surface. Figures 7 through 9 show the distributions of the optical path difference and the fast axis for the rotation angle $\theta =$ 0, 30 and 60˚, respectively. The <001> direction of the crystal is expressed by the black solid line in these figures. The unit of the optical path difference is nm/cm. In the figures of the fast axis distribution, the birefringence is represented by vector notation. The direction of vector expresses the fast axis direction and the length of vector expresses the optical path difference. It is found from these figures that the distribution of the optical path difference changes its shape with the rotation angle. On the other hand, the magnitudes of the optical difference are almost the same for all rotation angles.

Figures 10 through 12 show the distributions of the optical path difference and the fast axis obtained by the experiment. In this experiment, we used the birefringence measurement system EXICOR 150AT manufactured by HINDS instruments, Inc. In Figs. 10(b), 11(b) and 12(b), the vectors express only the direction of fast axis, and do not express optical path difference as Figs. 7(b), 8(b) and 9(b). It is found from the analysis results shown in Figs. 7 through 9 and the experimental results shown in Figs. 10 through 12 that the analysis results agree very well with the experimental results both for the optical path difference and for the fast axis.

We consider the optimum condition of the incident light from efficient aspect. The incident light should be polarized in the direction parallel to the plane of incidence, in other words $u_1 - u_3$ plane in Fig. 5. This is because it has only p-polarization component and does not reflect at Brewster's angle of incidence. In this case, polarizing direction of the light passing through the window corresponds to the u_1-axis in the $u_1 - u_2$ plane. The polarized light is resolved into two lights, the polarizing directions of which are fast axis and slow axis respectively. When the fast axis coincides with either the u_1-axis or the u_2-axis, the light is not resolved, the birefringence does not occur and the optical path difference becomes zero. For example, in Figs. 9(b) and 12(b), when the rotation angle $\theta = 60$˚, the fast axis in the area near the center almost corresponds to the u_1-axis or the u_2-axis. Judging from Figs. 7 through 12, we can say from this reason that the optimum rotation angle is 60˚ among three cases of rotation angle.

The distributions of optical path difference and fast axis obtained by the analysis agree with experimental results. The analytical prediction that the optimum rotation angle is 60˚ among three cases of rotation angle, $\theta = 0$, 30 and 60˚, is verified by

the experiment. The present simulation method provides a useful tool for designing laser equipments with CaF_2 single crystal as a window material.

(a) Optical path difference   (b) Fast axis
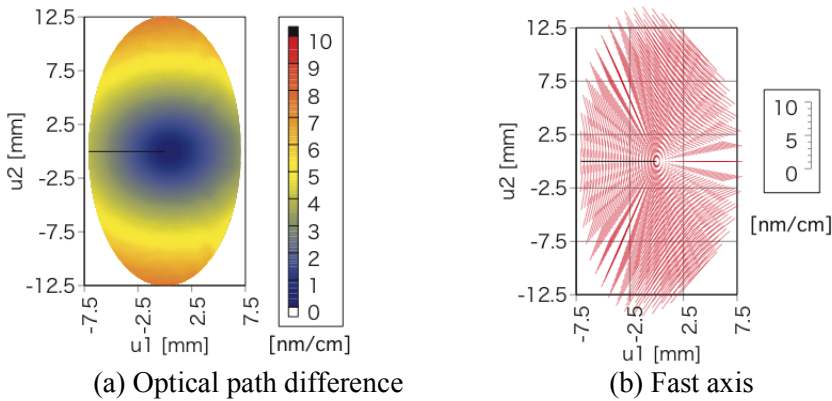
Figure 7: Analysis results of birefringence for $\theta = 0°$

(a) Optical path difference   (b) Fast axis
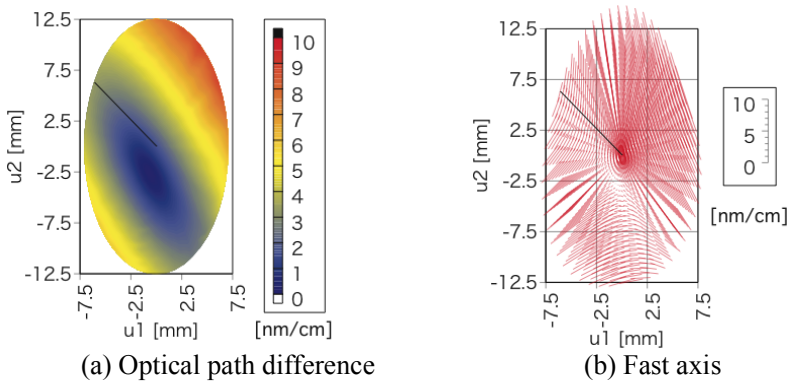
Figure 8: Analysis results of birefringence for $\theta = 30°$

6   Conclusion

We developed an analysis system for simulating birefringence of CaF_2 single crystal used as a chamber window of a gas laser light source caused by the mechanical stress due to holding loads and gas pressure. We performed the analyses for a single crystal slab with the surface vertical to the <111> direction of the crystal, using this

(a) Optical path difference (b) Fast axis
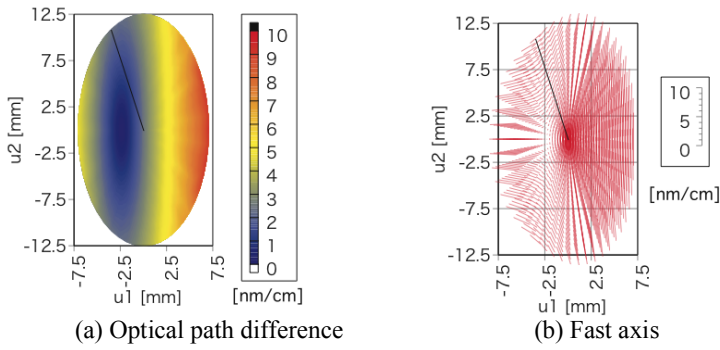
Figure 9: Analysis results of birefringence for $\theta = 60°$

(a) Optical path difference (b) Fast axis
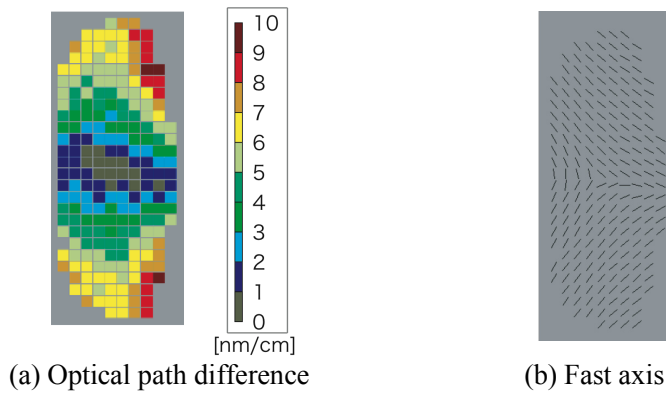
Figure 10: Experimental results of birefringence for $\theta = 0°$

(a) Optical path difference (b) Fast axis
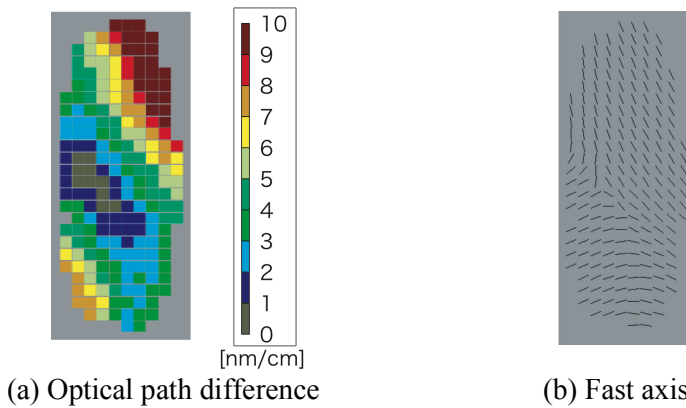
Figure 11: Experimental results of birefringence for $\theta = 30°$

(a) Optical path difference   (b) Fast axis
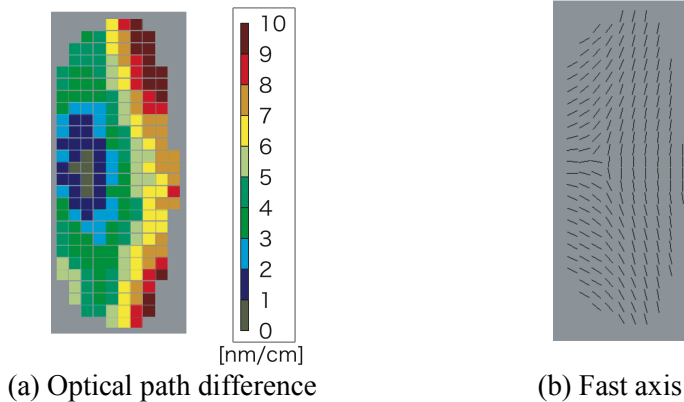
Figure 12: Experimental results of birefringence for $\theta = 60°$

analysis system. It is found from the result of stress analysis that the dominant factor for the stress in the single crystal window is the bending moment caused by the difference of pressure between laser gas and purge gas. In the birefringence analysis, we dealt with the Brewster's angle of incidence. The distributions of the optical path difference and the fast axis calculated from the present method agree well with those of the experiment for the respective rotation angles, $\theta = 0$, 30 and 60°. It is also found that the optimum rotation angle is 60° among three cases of rotation angle. The present method provides a useful tool for designing laser equipments with CaF_2 single crystal as a window material.

References

Abbott, J.; Wang, L.; Price, M.; Allan, D.; Slater, I. (2003): Prediction of CaF_2 Optical Properties from Thermal-Stress Models. *Proceedings of the 4th International Symposium on 157nm Lithography*.

Brocks, W.; Qi, W. (2002): Numerical Investigation of Creep Damage Development in the Ni-Based Superalloy IN 738 LC at 850°. *CMES: Computer Modeling in Engineering & Sciences*, vol. 3, no. 3, pp. 313-320.

Kliger, D. S.; Lewis, J. W.; Randall, C. E. (1990): *Polarized Light in Optics and Spectroscopy*, Academic Press, San Diego, p. 59.

Mittal, S. (2008): Linear Stability Analysis of Time-Averaged Flow Past a Cylinder. *CMES: Computer Modeling in Engineering & Sciences*, vol. 27, no. 2, pp. 63-78.

Miyazaki, N.; Ogino, H.; Kitamura, Y.; Mabuchi, T.; Nawata, T. (2009): Bire-

fringence Simulation of Annealed Ingot of Calcium Fluoride Single Crystal (Consideration of Creep Behavior of Ingot During Annealing Process). *Proceedings of SPIE, Optical Microlithography XXII*, vol. 7274, pp. 7274-151.

MSC Software (2007): *MSC Marc Vol. A, Theory and User Information*, Version 2007.

Nishioka, T.; Stan, F. (2003): A Hybrid Experimental-Numerical Study on the Mechanism of Three-Dimensional Dynamic Fracture. *CMES: Computer Modeling in Engineering & Sciences*, vol. 4, no. 1, pp. 119-139.

Nye, J. F. (1985): *Physical Properties of Crystals*, Clarendon Press, Oxford, p. 235.

Ogino, H.; Miyazaki, N.; Mabuchi, T.; Nawata, T. (2008): Birefringence Simulation of Annealed Ingot of Calcium Fluoride Single Crystal. *J. Crystal Growth*, vol. 310, pp. 221-228.

Ren J. (2008): Elastic Instability of Pseudo-Elastic Rubber Balloons, *CMC: Computers, Materials, & Continua*, Vol. 7, No. 1, pp. 25-32.

Schmid, M.; Weber, R.; Graf, T.; Roos, M.; Weber, H. P. (2000): *IEEE J. Quantum Electron,* vol. 36, pp. 620-626.

Schott Lithotec: *Calcium Fluolide Catalog*.

Vidal, M. D. (1974): *Comptes Rendus Hebdomadaires des Seances de l Academie des Sciences Serie B*, vol. 279, pp. 345-347.